Control Engineering Practice 71 (2018) 1–9

Contents lists available at ScienceDirect

Control Engineering Practice

journal homepage: www.elsevier.com/locate/conengprac

Applicability of available Li-ion battery degradation models for system and control algorithm design

Xing Jin [a], Ashish Vora [a], Vaidehi Hoshing [a], Tridib Saha [b], Gregory Shaver [a,*], Oleg Wasynczuk [b], Subbarao Varigonda [c]

[a] School of Mechanical Engineering, Purdue University, 585 Purdue Mall, West Lafayette, IN 47907, USA
[b] School of Electrical and Computer Engineering, Purdue University, 465 Northwestern Ave., West Lafayette, IN 47907, USA
[c] Cummins Inc., Columbus, IN 47202, USA

ARTICLE INFO

MSC:
00-01
99-00

Keywords:
Battery degradation models
Electrochemical model
Semi-empirical model
Empirical model
System design
Control design
Commercial A123 2.3 Ah graphite/$LiFePO_4$ cell

ABSTRACT

Within electrified vehicle powertrains, lithium-ion battery performance degrades with aging and usage, resulting in a loss in both energy and power capacity. As a result, models used for system design and control algorithm development would ideally capture the impact of those efforts on battery capacity degradation, be computationally efficient, and simple enough to be used for algorithm development. This paper provides an assessment of the state-of-the-art in lithium-ion battery degradation models, including accuracy, computational complexity, and amenability to control algorithm development. Various aging and degradation models have been studied in the literature, including physics-based electrochemical models, semi-empirical models, and empirical models. Some of these models have been validated with experimental data; however, comparisons of pre-existing degradation models across multiple experimental data sets have not been previously published. Three representative models, a 1-d electrochemical model (a combination of performance model and degradation model), a semi-empirical degradation model (the performance is predicted by an equivalent circuit model) and an empirical degradation model (the performance is predicted by an equivalent circuit model), are compared against four published experimental data sets for a 2.3-Ah commercial graphite/$LiFePO_4$ cell. Based on simulation results and comparisons to experimental data, the key differences in the aging factors captured by each of the models are summarized. The results show that the physics-based model is best able to capture results across all four representative data sets with an error less than 10%, but is $20x$ slower than the empirical model, and $134x$ slower than the semi-empirical model, making it unsuitable for powertrain system design and model-based algorithm development. Despite being computationally efficient, the semi-empirical and empirical models, when used under conditions that lie outside the calibration data set, exhibit up to 71% error in capacity loss prediction. Such models require expensive experimental data collection to recalibrate for every new application. Thus, in the author's opinion, there exists a need for a physically-based model that generalizes well across operating conditions, is computationally efficient for model-based design, and simple enough for control algorithm development.

1. Introduction

Vehicle electrification offers the potential to decrease fuel use, greenhouse gas emissions, and tailpipe emissions of criteria pollutants. Batteries play an important role in electrified propulsion systems. Lithium ion batteries have the advantage of high energy density, high power density, and low self-discharge rate (Oswal, Paul, & Zhao, 2010). These favorable properties, as well as decreasing costs, have made them the most popular technology for automotive applications (Safari & Delacourt, 2011b; Wang et al., 2011).

In spite of these favorable properties of lithium ion batteries, aging and degradation during usage remain an impediment to widespread adaption. Loss of cyclable lithium via side reactions, loss of electrode active material, and resistance increase through interfacial layer growth or contact issues are among the most common aging phenomena encountered in lithium ion batteries (Delacourt & Safari, 2012). The

* Corresponding author.
E-mail address: gshaver@purdue.edu (G. Shaver).

https://doi.org/10.1016/j.conengprac.2017.10.002
Received 22 February 2017; Received in revised form 3 October 2017; Accepted 5 October 2017
Available online 4 November 2017
0967-0661/

rate of capacity loss for each mechanism is a complex nonlinear process dependent on various factors including temperature, state of charge (SOC), depth of discharge (DOD), C-rate, and storage condition of the battery.

Several types of models for predicting battery degradation have been widely used in hybrid electric vehicle system-level study, including physics-based electrochemical models (Jin et al., 2017c; Lawder, Northrop, & Subramanian, 2014; Prada et al., 2013; Vora et al., 2015), semi-empirical models (Smith, Markel, & Pesaran, 0000), and empirical models (Peterson, Apt, & Whitacre, 2010; Vora et al., 2017; Wang et al., 2011). These models describe the dependence of battery resistance and capacity fade on various aging factors (Jin, 2017; Smith, Earleywine, Wood, Neubauer, & Pesaran, 2012; Smith et al., 0000). Due to their simplicity and sufficient accuracy for many applications, semi-empirical and empirical models have been used for on-line state-of-health (SOH) estimation. As will be shown, the usability of these models, however, is generally limited to operating conditions characteristic of the data used for calibration. To cover a relatively wide range of operating conditions, expensive and time consuming experiments need to be conducted. In contrast, electrochemical models, which describe aging phenomena with some physical basis, have the potential to allow the analysis to be extended to a larger range of operation conditions once the model is calibrated, but are computationally more expensive than the aforementioned empirical and semi-empirical models.

A semi-empirical degradation model developed by National Renewable Energy Laboratory (NREL) (Smith et al., 0000, 2013) was generated by compiling experimental data under different aging conditions from multiple sources. Reference (Wang et al., 2011) proposed an empirical model that was fitted to experimental data with variable temperatures, C-rates and DODs. Reference (Onori, Spagnol, Marano, Guezennec, & Rizzoni, 0000) presented a weighted ampere-hour throughput model based on a severity factor map that captures the battery degradation due to the different operating factors including temperature and C-rate. Several physics-based aging models for lithium-ion batteries have also been described in the literature. In Safari, Morcrette, Teyssot, and Delacourt (2009) and Delacourt and Safari (2012), an aging model based on the single-particle approach was developed to take into account the solid-electrolyte-interface (SEI) layer thickness growth and possible active material loss at both anode and cathode. A correlation of graphite active material loss as a function of C-rate and temperature was implemented to get better agreement with experimental data. Reference (Prada et al., 2013) showed a simplified isothermal physics-based aging model, in which the SEI layer growth was related to both capacity loss and internal resistance increase. However, to the best of the authors' knowledge, none of these models have been compared with each other and with multiple experimental datasets spanning various operating conditions.

The objective of this paper is to help model users understand the strengths and weaknesses of these different types of degradation models and thus select the most appropriate model, if available, for their specific application. As will be shown, the higher fidelity degradation model described by the electrochemical model relies on the performance information, i.e. solid/electrolyte phase potential, solid/electrolyte concentration, and current density. The two degradation mechanisms described by ordinary differential equations (ODEs) are easy to solve, but the inputs to those ODEs require solving the electrochemical performance model. It should be highlighted that several authors proposed different ways to simplify the performance model, including Padé approximation (Forman, Bashash, Stein, & Fathy, 2011), residue grouping (Smith, Rahn, & Wang, 2008), polynomial approximation (Subramanian, Diwakar, & Tapriyal, 2005), Galerkin projection (Fan, Pan, Canova, Marcicki, & Yang, 2016), etc., however, none of them include degradation model simplification, computational complexity, or accuracy considerations. The semi-empirical and the empirical degradation models, on the other hand, do not need detailed knowledge of the electrochemical system, which is an advantage of these simpler models. The inputs for these models, i.e. current, SOC, voltage, can be obtained by the equivalent circuit model, the electrochemical model, or experimental data.

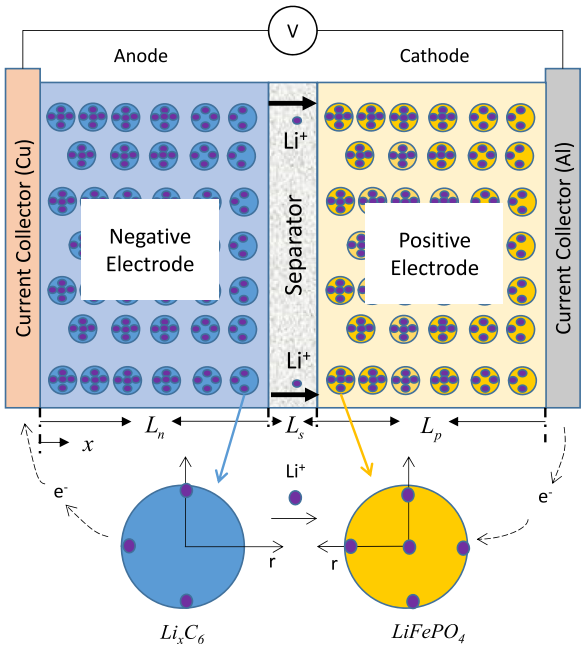

Fig. 1. Schematic of a Li-ion battery (graphite/$LiFePO_4$), with a separator between two electrodes (anode and cathode) (Smith & Wang, 2006).

A commercial graphite/$LiFePO_4$ (LFP) cell, a promising technology for automotive applications due to its excellent chemical and thermal stability and low cost (Wang et al., 2011), is taken as an example to illustrate the differences. This paper is organized as follows: Section 2 describes three battery degradation models, including a 1-D electrochemical model, a semi-empirical model, and an empirical model. Section 3 presents the model-to-model and model-to-data comparisons, and some discussion of these results. It also describes the tradeoff between accuracy and computational time for the 1-D electrochemical model. Finally, Section 4 concludes the paper with some key takeaways.

2. Battery degradation models

A schematic diagram of a typical graphite/$LiFePO_4$ (LFP) cell with a single pair of porous electrodes is shown in Fig. 1 (Smith & Wang, 2006). As shown, the model includes three domains: negative electrode (anode), separator, and positive electrode (cathode). During discharge, Li ions (represented as purple dots) diffuse to the surface of the LiC_6 active material particles within the anode, de-insert from the surface, and then transfer into the electrolyte solution. These lithium ions travel through the electrolyte solution and separator to the cathode, and diffuse towards the inner regions of the $LiFePO_4$ active material particles. The separator is an ionic conductor and electronic insulator, which forces the electrons to flow through an external circuit. The reverse occurs during the charging process.

Along with the charge and discharge operations, aging or degradation phenomena also occur inside a battery, including capacity fade, power fade, stress–strain effects, and mechanical degradation. For each type of degradation model i.e. physics-based, semi-empirical and empirical, there are many models available. AutoLion ST is a commercially available 1-D electrochemical model, which is implemented as a software-in-the-loop model block. It has been validated across different chemistries under different operating conditions (Kalupson, Luo, & Shaffer, 2013; Vora et al., 2015, 2017). Different semi-empirical and empirical models published in the literature are calibrated for different

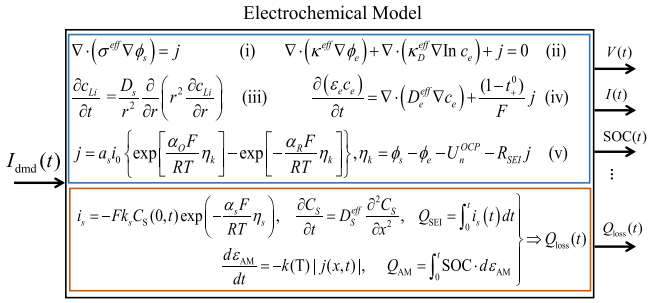

Fig. 2. Schematic diagram of the degradation model input and output (Jin et al., 2017b; Kalupson et al., 2013). Equations (i) and (ii) represent the conservation of charge in the solid phase and electrolyte phase, (iii) represents the Li-ion diffusion in active material particle, (iv) gives the species conservation in the electrolyte, and (v) is the Butler–Volmer equation.

cells, i.e. different anode/cathode geometry, different design, different chemistry, etc. Three pre-existing aging models which are calibrated for A123 26650 LFP/graphite cell and are widely referenced are chosen for comparison in this paper. A123 26650 LFP/graphite cell is taken as example chemistry due to the availability of models calibrated for this cell and the availability of degradation data for this cell. These models will be discussed in the rest of this section.

2.1. 1-D electrochemical model — ALST model

AutoLion ST (version 5.2.1 is used in this paper) is a thermally-coupled-electrochemical model developed by EC Power that is intended to predict battery performance (current, voltage, state-of-charge (SOC), etc.) and degradation (Kalupson et al., 2013). From here on, this electrochemical model will be called the 'ALST model' for simplicity. The inputs and outputs of this ALST model are shown in Fig. 2. The battery performance, i.e. voltage, current, state of charge (SOC), is predicted by Equations (i)–(v), which are the constitutive laws used in most of the electrochemical models to predict the Li-ion transportation. These five governing equations are called the performance model in this study. In addition, there are two degradation mechanisms coupled to this model: loss of active material and SEI layer growth (Eqs. (1) and (2), as described below).

Active material loss. The active material undergoes volume and structural changes during uptake and removal of lithium ions. These changes cause mechanical stress in the particle structure potentially resulting in cracks or structural damage, gradually isolating active material (AM) during cycling. As a result, the amount of cyclable lithium is reduced, which leads to loss of cell capacity. Since the active material isolation is a consequence of the lithium intercalation process, an equation that relates isolation rate to intercalation current is used in ALST (Kalupson et al., 2013):

$$\frac{d\varepsilon_{\mathrm{AM}}}{dt}=-k(T)|j(x,t)| \tag{1}$$

where $\varepsilon_{\mathrm{AM}}$ is the volume fraction of active material, $k(T)$ is a temperature-dependent rate coefficient, and $j(x,t)$ is the current density at location x. A schematic of the discretized elements and the current density distribution within a cell is shown in Fig. 3. For the ith element in the anode or cathode, $j(x,t)$ is denoted by $j_{a/c,i}^{Li}$.

SEI layer growth. The SEI layer is formed and grows over time as a product of irreversible side reactions between electrode and electrolyte materials. Li-ions are consumed in these irreversible side reactions and this results in capacity loss. The SEI layer growth is captured via the following equation (Kalupson et al., 2013):

$$\frac{d\delta_{\mathrm{SEI}}}{dt}=-\frac{i_s}{2F}\frac{M_{\mathrm{SEI}}}{\rho_{\mathrm{SEI}}} \tag{2}$$

where F is the Faraday constant, M_{SEI} and ρ_{SEI} are the molecular weight and density of the SEI layer, respectively, and i_s is the side reaction current density (based on reaction surface area). In this model, side reaction current density is described using a Tafel-like kinetic equation (Kalupson et al., 2013):

$$i_s=-Fk_s c_{\mathrm{EC}}^s\exp\left[-\frac{\beta F}{RT}\left(\phi_s-\phi_e-U_{\mathrm{SEI}}-R_{\mathrm{SEI}}i_t\right)\right] \tag{3}$$

where k_s is the rate constant, a tunable parameter for calibration, β is the charge transfer coefficient, R is the ideal gas constant, T is temperature, ϕ_s is the solid phase potential, ϕ_e is the electrolyte potential, U_{SEI} is the open circuit potential of the side reaction, R_{SEI} is the resistance of SEI layer, and c_{EC}^s is the ethylene carbonate (EC) concentration at the reaction surface. In this degradation model, only the ethylene carbonate (EC) related side reaction is considered in ALST. i_t is the total current density of both lithium intercalation and side reaction, and under storage conditions $i_s=i_t$.

It should be highlighted that Eqs. (1) and (2) are only two first-order ODEs, however, to solve them requires solving a complex set of governing equations across the thickness of the anode or cathode, i.e. ϕ_s in conservation equation of charge in electrode, ϕ_e in conservation equation of charge in electrolyte, $j(x,t)$ in Butler–Volmer equations, etc. It is not possible to solve the degradation equations without solving the electrochemical performance model.

As suggested by Delacourt and Safari (2012) and Jin et al. (2017a), the SEI layer growth sub-model is first calibrated using experimental data from aging tests under storage conditions. Experimental data from aging tests under cycling conditions is then used to calibrate the active material loss sub-model. The cell capacity in ALST model is determined by a capacity characterization process. In this process the cell is fully charged to high cutoff voltage, and then discharged with a 0.5C constant current until it reaches the low cutoff voltage. The discharge capacity is defined as the cell capacity.

2.2. Semi-empirical degradation model

A physically-motivated semi-empirical battery lifetime model was developed by the National Renewable Energy Laboratory (NREL) (Smith et al., 0000, 2013). From here on this model will be referred to as the 'semi-empirical model'. In this model, observable degradation mechanisms were represented by low-order surrogate models, and the parameters for these surrogate degradation models were fitted to experimental battery aging data. The inputs for this degradation model is generally provided by an equivalent circuit model (Smith et al., 2012).

Two degradation mechanisms were captured for the A123 26650 $LiFeO_4$ cell: (i) internal resistance increase, which has a direct impact on the maximum power that the cell can source or sink, and (ii) reduction in capacity. Both models depend on calendar life and the number of charge/discharge cycles that the battery has undergone. The calendar-related fade that is captured in this model is attributed to growth of a resistive SEI layer at the electrode surface. SEI layer formation increases cell resistance and consumes cyclable Li-ions. The model assumes that the calendar-driven resistance growth and capacity fade are proportional to square root of time (Ploehn, Ramadass, & White, 2004; Smith et al., 2012). As mentioned previously, cycle-driven fade is generally attributed to mechanical expansion/contraction of electrodes resulting in stress/deformation and fracture. This mechanical stress/deformation results in loss of electrode active sites, which leads to capacity fade and resistance growth. The semi-empirical model assumes that capacity fade and resistance growth due to cycling are proportional to the number of cycles. To capture the number of micro-cycles at different DOD levels, a rainflow counting algorithm is used (Niesony, 2009).

The life model assumes that internal resistance growth (R_{int}) due to calendar-driven and cycling-driven mechanisms can be predominantly additive.

$$R_{\mathrm{int}}=a_0+a_1t^{\frac{1}{2}}+\frac{a_2}{Q_{\mathrm{site}}}-a_3\left[1-\exp\left(-\frac{t}{200}\right)\right] \tag{4}$$

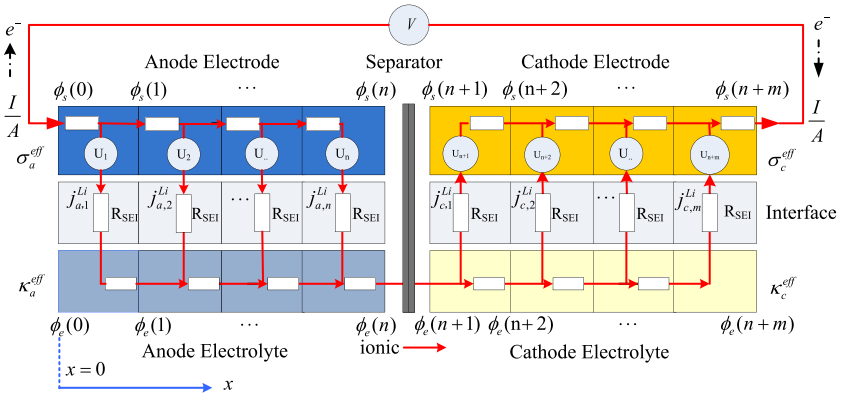

Fig. 3. Schematic showing the 1-D discretization used in the AutoLion lithium ion battery cell model. There are n elements in the anode and m elements in the cathode. Subscripts a and c stand for anode and cathode, respectively. Subscript number i stands for ith element. For example, $j^{Li}_{a,1}$ is the current density at the first element in anode. ϕ_s is solid phase potential, ϕ_e is electrolyte potential, R_{SEI} is the resistance of SEI layer.

Table 1
Equation to predict capacity fade at a given discharge rate (Wang et al., 2011).

C-rate	Life model
C/2	$Q_{loss} = 30330 \cdot \exp(\frac{-31500}{RT}) \cdot (Ah)^{0.552}$
2C	$Q_{loss} = 19330 \cdot \exp(\frac{-31000}{RT}) \cdot (Ah)^{0.554}$
6C	$Q_{loss} = 12000 \cdot \exp(\frac{-29500}{RT}) \cdot (Ah)^{0.56}$
10C	$Q_{loss} = 11500 \cdot \exp(\frac{-28000}{RT}) \cdot (Ah)^{0.56}$

Cell capacity (Q) is assumed to be controlled by either loss of cyclable Li or loss of active sites, which can be represented by:

$$Q = \mathbf{min}(1, Q_{Li}, Q_{site}) \tag{5}$$

where Q_{Li} is called the cyclable lithium-ion-limited relative capacity, and $1 - Q_{Li}$ is the relative capacity fade due to cyclable lithium ion loss. Similarly, Q_{site} is the site limited relative capacity, and $1 - Q_{site}$ is the relative capacity fade due to active site loss.

$$Q_{Li} = b_0 - b_1 t^{\frac{1}{2}} - b_2 \left[1 - \exp(-\frac{t}{200})\right]$$

$$Q_{site} = [c_0^{1+p} + c_1 c_0^p (1+p) N]^{\frac{1}{1+p}}$$

where N is the number of micro-cycles, t is the calendar time, a_0, a_1, a_2, a_3, b, b_1, b_2, c_0, c_1, and p are fitted parameters. These fitting parameters are described with functional dependence on operating conditions, i.e. DOD, C-rate, temperature, and so on. For more details, please refer to Smith et al. (2013). Capacity fade data from multiple sources, including Safari & Delacourt (2011a) and Wang et al. (2011), and some other test data sets, are used to tune the model.

2.3. Empirical degradation model — Regression model

Empirical models use available experimental data to predict the future behavior of lithium-ion batteries without detailed knowledge of the electrochemical cell design. Polynomial, exponential, power law, logarithmic, and trigonometric functions are commonly used as empirical models (Ramadesigan et al., 2012). The computational simplicity of empirical models generally enables faster computations.

A popular empirical model for the A123 26650 LFP cell that has been cited and used in several studies is the one developed in Wang et al. (2011). In that paper, four experimental parameters — time, temperature, DOD, and discharge-rate are investigated. For each discharge-rate, a least squares regression model Eq. (6) is established to capture the capacity loss.

$$Q_{loss} = B \cdot \exp\left(-\frac{E_a}{RT}\right)(Ah)^z \tag{6}$$

where B, E_a and z are fitting parameters. It can be seen that this model combined various factors (e.g. time, temperature, DOD) into an Ah-throughput-dependent (ampere-hour throughput is defined as: number of cycles × DOD × full cell capacity) aging expression. B, E_a and z are obtained from least-square fits with the experimental data from (Wang et al., 2011), and the fitted models are summarized in Table 1. For simplicity, this empirical life model will be referred to as the 'regression model' in the later sections. Since the regression model is provided only for 0.5C, 2C, 6C, and 10C, capacity loss at other C-rates is estimated by interpolation/extrapolation.

3. Simulation results

In this section, the three models will be compared to one another and four experimental datasets (all of them are for a 2.3 Ah A123 26650 LFP cell) from the literature (Nagpure, 2013; Safari & Delacourt, 2011a; Spagnol, Onori, Madella, Guezennec, & Neal, 2010; Wang et al., 2011). For more details about these experimental data sets, please refer to Nagpure (2013), Safari and Delacourt (2011a), Spagnol et al. (2010) and Wang et al. (2011). Reference (Safari & Delacourt, 2011a; Spagnol et al., 2010) use data that is representative of typical EV and HEV dynamic drive cycles, respectively. Nagpure (2013) uses a 16C constant current charge/discharge profile, which is used to test if the degradation models are predictive under conditions consistent with large electrified vehicles.

As shown in Table 2, the regression model was calibrated using data set 2, and the semi-empirical model with data sets 2 and 3. Data sets 2 and 3 have relatively low C-rates and constant-current charge/discharge profiles. The ALST model was calibrated using the capacity loss under storage condition and 1C constant-current charge/discharge profile (Safari & Delacourt, 2011a), which were not the same as Data Set 3, but again, only using low C-rate and constant-current charge/discharge profiles. It is therefore highly desirable to compare these three models against some data sets with high C-rates and dynamic drive cycles. This is accomplished in Sections 3.1 and 3.4 using data sets 1 and 4. The inputs for the semi-empirical and empirical models, i.e. current, SOC, voltage, are provided by a first order equivalent circuit model (ECM) as suggested by Jin et al. (2017a), Smith et al. (2012) and Vora et al. (2017).

3.1. Experimental data set 1 — representative of HEV duty cycle

Reference (Spagnol et al., 2010) describes a synthetic current profile (Fig. 4(a)), created such that the aging factors i.e. initial SOC, DOD, and C-rate distribution are representative of a typical HEV application. This current cycle was repeated to cycle the cell at 45 °C until it reached end-of-life (EOL), which was defined as 20% of cyclable capacity loss.

Table 2
Data sets used in model validation or calibration.

Data sets	ALST model	Semi-empirical model	Regression model
Data set 1 (Spagnol et al., 2010)	Validation	Validation	Validation
Data set 2 (Wang et al., 2011)	Validation	Calibration	Calibration
Data set 3 (Safari & Delacourt, 2011a)	Validation	Calibration	Validation
Data set 4 (Nagpure, 2013)	Validation	Validation	Validation

Table 3
Model comparison for computational time (30 000 cycles).

Battery models	ALST model	ECM + Semi-empirical model	ECM + Regression model
Computational time	2400 s	17.9 s	122.4 s

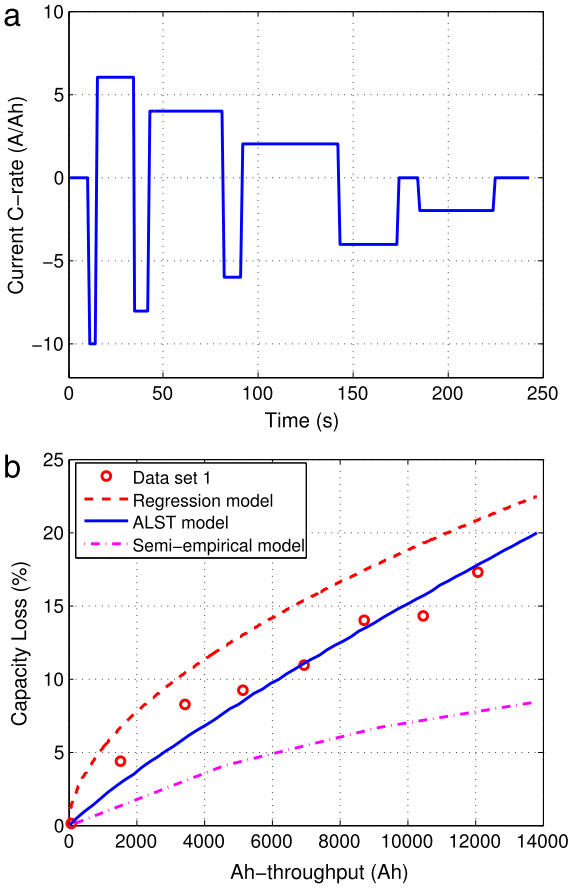

Fig. 4. Experimental data set 1. (a) is the synthetic current profile, which is representative of actual HEV operation (Data Set 1 Spagnol et al., 2010). Sign convention: positive is discharging the battery, negative is charging the battery. Ah-throughput per cycle = 0.48 Ah. (b) shows the simulation result vs. experimental data set 1 (Spagnol et al., 2010). Solid line is ALST simulation result, dash line is the result of regression model, and dash–dot line is the result of semi-empirical model. Ah-throughput = Number of Cycles × Ah-throughput per cycle.

The capacity loss predicted by each of the three models for the cell cycled with this synthetic current profile is shown in Fig. 4(b) as a function of Ah-throughput. The ALST model shows good agreement with the experimental data, outperforming both the semi-empirical and regression models. Computational times (including performance model and degradation model) for the three models are shown in Table 3. From Table 3, it can be seen that the semi-empirical model (the fastest one) is 134 times faster than the ALST model (T_s = 1 s, mesh number in anode, separator, and cathode is 2, 2, and 2, respectively).

Table 4
AutoLion ST computational time vs. accuracy.

Number of meshes (anode-separator-cathode)		8-5-8	4-2-4	2-2-2
Computational time (s/cycle)	T_s = 0.1 s	6.09	1.50	0.41
	T_s = 0.5 s	3.14	0.58	0.15
	T_s = 1.0 s	1.58	0.43	0.08
Percentage error (%)	T_s = 0.1 s	0%	0%	0%
	T_s = 0.5 s	0.27%	0.27%	0.40%
	T_s = 1.0 s	1.62%	1.62%	1.75%

Computational cost vs accuracy tradeoff in ALST model. All of the simulations were executed on the same computer with a Core i5-4590 3.3-GHz, 8-GB memory. The computational cost for the 1-D electrochemical model is initially much higher than the other two models. Two ways to speed up the simulation are available within ALST: (i) use fewer zones for the anode, separator, and cathode (Fig. 3 shows how the zones are defined), and/or (ii) run the simulation with a larger simulation time step. However, both strategies could result in a decrease in accuracy. It is therefore desirable to study the tradeoff between accuracy and computational cost with a two parameter design-of-experiments (DOE). The results are listed in Table 4. In the ALST model, the default number of zones used is 8-5-8 (anode-separator-cathode), which corresponds to 8 zones for the anode, 5 zones for the separator, and 8 zones for the cathode. A 2-2-2 (anode-separator-cathode) zone arrangement is the minimum number of zones required by ALST to provide a reasonable result. As shown in Table 4, three levels of sampling time are considered, 0.1, 0.5, and 1 s. The maximum frequency of the HEV cycle is 0.33 Hz. The Nyquist sampling criterion requires that the sampling frequency be greater than twice the maximum frequency contained in the signal, to capture the complete information. Thus, the sampling frequency has to be greater than 0.67 Hz, and sampling time T_s should be less than 1.5 s.

The finest mesh (8 nodes in the anode and cathode, and 5 zones in separator) and smallest sampling time (T_s = 0.1 s) simulation result is used as the truth reference (Q_{ref}) in the accuracy comparison. Percentage error is defined as the percentage difference of the capacity loss at the ending point of the simulation:

$$\text{Percentage error} = \frac{|Q_{\text{ref}} - Q_{\text{loss}}|}{Q_{\text{ref}}} \times 100\% \tag{7}$$

where Q_{loss} and Q_{ref} are the cell capacity loss and the reference cell capacity loss at the end of 30 000 cycles, respectively.

Table 4 shows the tradeoff between computational time and accuracy. It can be seen that the simulation with largest sampling time and least number of meshes shows the worst accuracy and fastest speed (30 times faster than the reference case). The results of the truth reference solution and the fastest simulation, cycled by the current profile shown in Fig. 4(a), are shown in Fig. 5, and both cases show good agreement with the experimental data. As such, the computational time can be reduced from 6.09 to 0.08 s/cycle without significant decrease in accuracy. To speed up the simulation, the grid mesh of 2-2-2 (anode-separator-cathode) and time step T_s = 1 s is used in all simulations

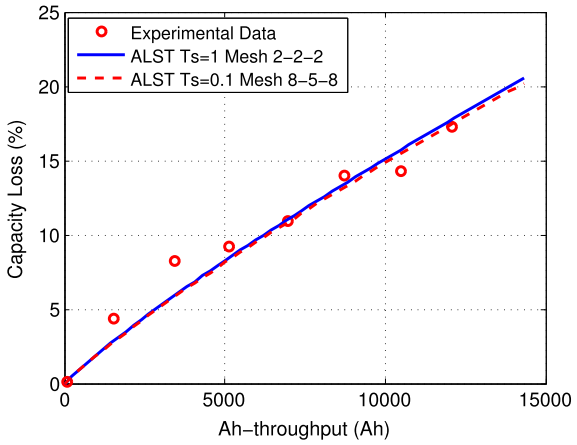

Fig. 5. Comparison of the truth reference case vs. fastest computational speed case. Dash line shows the truth reference Q_{ref} (Ts = 0.1 s Mesh 8-5-8), and solid line is the result with the fastest computational speed (T_s = 1 s Mesh 2-2-2).

in Section 3 (i.e. including the value for simulation time reported in Table 3). It should be noted that, even with this improvement, the ALST model takes up to 2400 s to simulate the battery performance and degradation until it reaches its end of life. For the system-level vehicle design and optimization, where a large number of different sizes of batteries must be analyzed over a wide range of operating conditions, this computational speed becomes a bottleneck.

3.2. Experimental data set 2 — low C-rate cycle under varying temperatures

In Wang et al. (2011), experimental data of a low C-rate (0.5C) cycle under different temperature conditions is reported. The regression model described in Section 2.3 and Wang et al. (2011), was calibrated using this data set as described in Wang et al. (2011). The cycling and capacity characterization procedure described in that paper is summarized as follows:

(1) The cell was de-rated to 2 Ah. As a result, the 1C current is 2 A. The high and low cutoff voltages were 3.6 V and 2.0 V, respectively.
(2) The cell was discharged with a constant current of 0.5C until the depth of discharge (DOD) is reached.
(3) The cell was charged with a constant current–constant voltage (CC–CV) protocol. A 0.5 C current was used to charge the battery to 3.6 V during the constant-current part. Subsequently, the voltage was held at 3.6 V until the current dropped below 0.1 A for a maximum of 2 days.
(4) The delivered discharge capacity and discharge time in Step 2 were saved for capacity-fade measurement. Steps 1–3 were repeated until the cell reached its EOL, which was defined as failing to deliver the required capacity before reaching a cell voltage of 2.0 V.

In Fig. 6, results of the capacity loss from all three models at different temperatures are compared with this experimental data set. In Wang et al. (2011), the authors claim that variation in DOD has negligible impact on degradation rate, and hence, DOD specific results are not shown. Instead, results across all DODs are lumped together.

Overall, all three models perform similarly, and capture with reasonable accuracy the impact of Ah-throughput and temperature, as shown in Fig. 6. The ALST and semi-empirical models capture the effect of DOD on degradation rate but in a surprisingly contradictory way. To understand this contradictory result, the two models are simulated under different average SOC and DOD conditions. Note that there is no experimental data available for these test conditions.

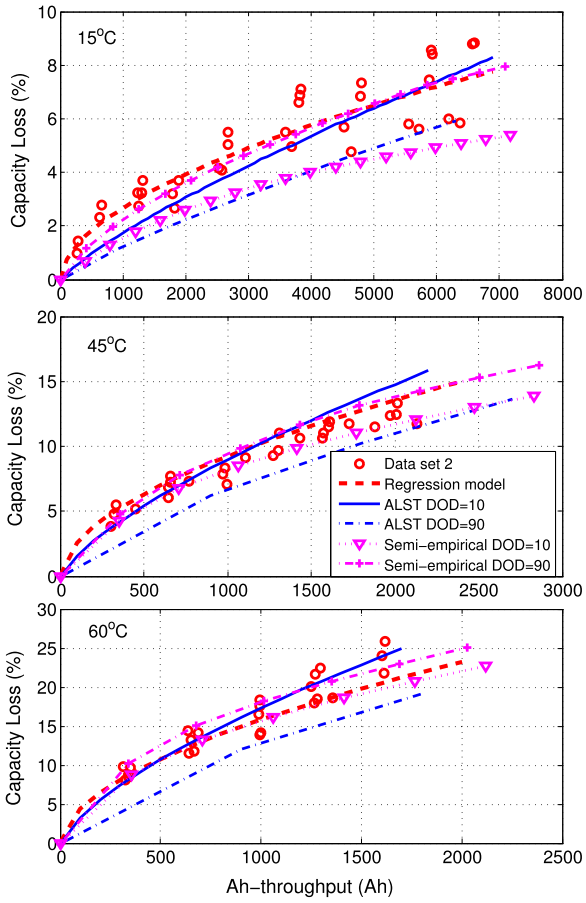

Fig. 6. Experimental capacity loss measured at three different temperatures (15 °C, 45 °C, and 60 °C), and corresponding simulation results. All DOD cases are combined in experimental data, and the DOD impact is ignored in the regression model. To test whether the DOD effect is captured, two DOD cases are shown for the AutoLion and semi-empirical models (DOD= 0.1 or 10%; DOD= 0.9 or 90%). Ah-throughput in Wang et al. (2011) was defined as A_h = Number of Cycles × DOD × Cell Capacity.

Impact of average SOC and DOD in ALST and semi-empirical models. Further simulations were run with the ALST model and the semi-empirical model varying average SOC and DOD one at a time to understand the impact that each of these separately has in the two models. Fig. 7 (a) shows each model exercised with two cycles, each of which have the same C-rate (0.5C) and DOD (10%) but different average SOCs. For the first cycle, SOC ranges from 30% to 40% (i.e. average SOC = 35%), and for the second cycle, SOC ranges from 70% to 80% (i.e. average SOC = 75%). Fig. 7 (a) shows that, with the same DOD, higher average SOC results in higher capacity loss in both models.

Fig. 7 (b) shows each model exercised with two cycles, each of which have the same C-rate (0.5C) and average SOC (75%) but different DODs. For the first cycle, SOC ranges from 55% to 95% (i.e. DOD = 40%), and for the second cycle, SOC ranges from 70% to 80% (i.e. DOD = 10%). Fig. 7 (b) shows that, with the same average SOC, DOD has no impact on degradation in the ALST model. However, in the semi-empirical model, higher DOD results in higher capacity loss.

Now going back to Fig. 6, because the upper bound of the SOC window is fixed for all DOD conditions in data set 2, a larger DOD implies a lower average SOC. For the ALST model this leads to slower degradation and capacity loss rate. For the semi-empirical model, however, there are competing effects. The larger DOD will increase degradation rate, but the lower average SOC will decrease degradation rate. In this case, it appears that the effect of DOD is dominant. From the experimental data in data set 2 (Fig. 6), it is not possible to determine which of these two models correctly captures the impact of DOD on degradation rate. To

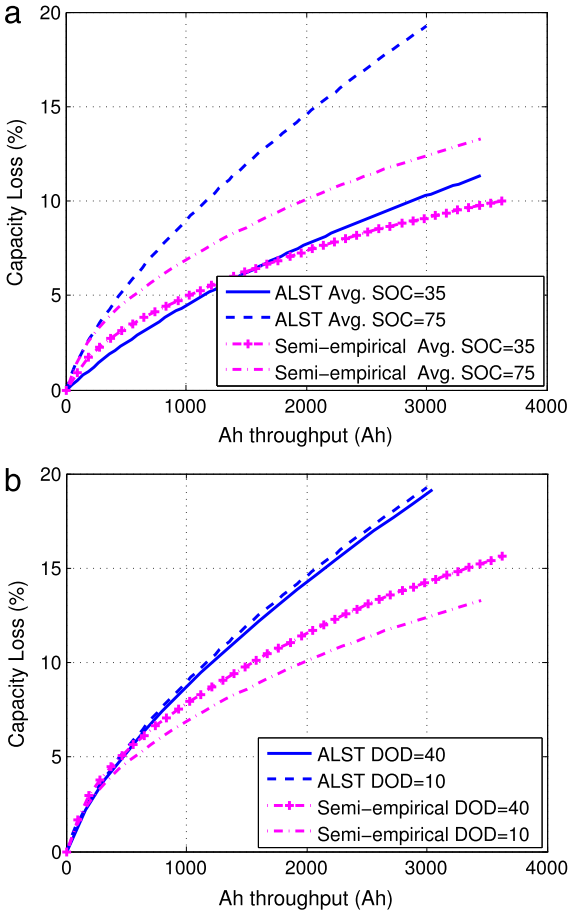

Fig. 7. The impact of average SOC and DOD on capacity loss captured in ALST and semi-empirical models. (a) shows the impact of average SOC on two models, and (b) shows the impact of DOD on two models.

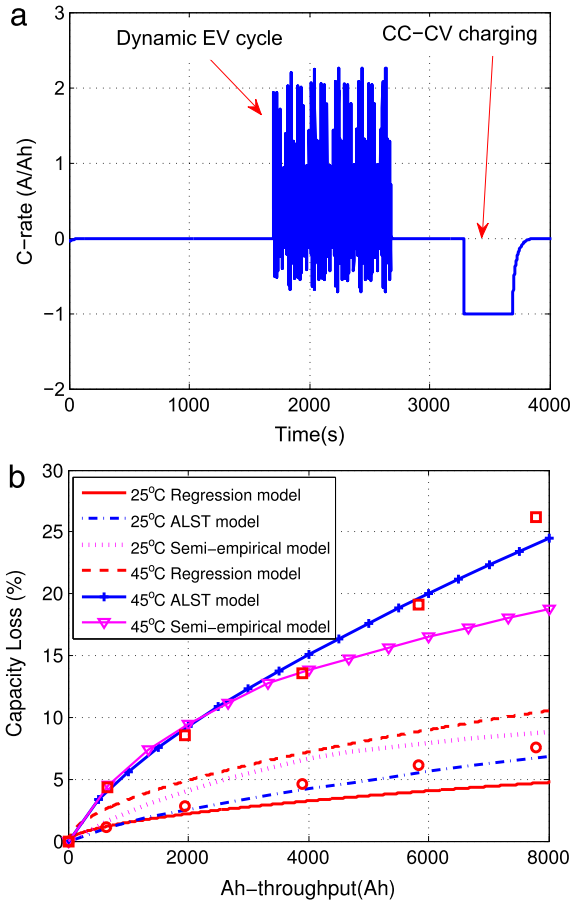

Fig. 8. Experimental data set 3. (a) shows the entire EV cycle (Safari & Delacourt, 2011a), and the sign convention is positive for discharge, negative for charge. (b) is the simulation vs experimental results under EV drive cycle. Dots are experimental data (Safari & Delacourt, 2011a), solid line is ALST simulation result, dashed line is the result of regression model, and dash–dot line is the result of semi-empirical model.

determine this, it is necessary to obtain experimental data under test conditions such as those depicted in Fig. 7. This knowledge could be critical in designing battery management algorithms.

3.3. Experimental data set 3 — representative of an electric vehicle (EV) cycle

The complex drive cycle from Safari and Delacourt (2011a), as shown in Fig. 8(a), is intended to represent a current profile consistent with an EV application. In this experiment, the cell was exercised as follows

(1) The cell was first charged with a CC–CV protocol (1C current for constant-current part, and then constant 3.6 V until the current drops below 0.1 A), after which it was left to rest for 30 min
(2) Discharged the cell down to 3 V using the dynamic power profile followed by a 10-min rest period.

This cycle was repeated continuously for one year and data was collected every 3 months. A comparison of experimental data and simulation results from the three models is shown in Fig. 8(b). At 25 °C, the simulation results from all three models correlate well with the experimental data, with the ALST model demonstrating the best predictions. At 45 °C, the simulation result of ALST shows the best match with the experimental data. The result of semi-empirical model shows agreement until the 6th month (corresponding to an Ah-throughput of approximately 4000 Ah), after which some discrepancy starts to appear. However, the regression model significantly underpredicts capacity loss. Note that this drive cycle includes a large rest period, and hence, the calendar aging component of capacity loss is expected to be more dominant. Since the regression model does not account for calendar life aging, it underpredicts the capacity loss. Calendar aging is exacerbated by high temperature, which can be seen in the increased error of the regression model at 45 °C as compared to 25 °C.

In summary, the physics-based ALST and semi-empirical models outperform the empirical model, in large part because the empirical model does not include a calendar-life aging component. Furthermore, the ALST model does a slightly better job correlating with the data than does the semi-empirical model, as would be expected, since the ALST model is physics-based.

3.4. Experimental data set 4 — high C-rate cycle

Reference (Nagpure, 2013) presents a set of experimental data in which the cell was cycled at 45 °C with a high C-rate of 16C from 45% to 55% SOC. In HEV applications, the maximum C-rates could reach this value, although for just a short time interval, for example, during an aggressive braking maneuver in a heavy vehicle. The current profile (Fig. 9(a)) used in simulations assumes a 100-s rest time in between cycles. Reference (Nagpure, 2013) assumed a 20% capacity loss as the definition of end of life, however, the cell capacity dropped dramatically after 29 500 cycles. A comparison of experimental data (up to 29 500 cycles) and the simulation results from all three models are shown in Fig. 9(b). The semi-empirical model underpredicts the capacity loss by 71%

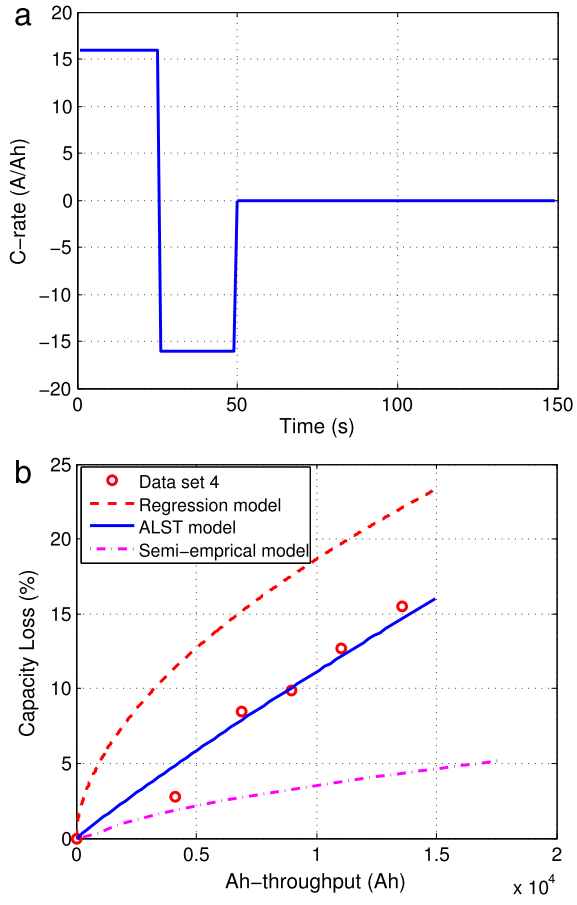

Fig. 9. Experimental data set 4. (a) shows the 16C constant current to cycle the cell between 45% to 55% SOC (Data Set 4 Nagpure, 2013). Ah-throughput per cycle = Cell capacity × 2 × DOD = 0.46 Ah. (b) shows the simulation result vs. experimental data from Data Set 4 (Nagpure, 2013). Solid line is ALST simulation result, dashed line is the result of regression model, and dash–dot line is the result of semi-empirical model. Ah-throughput = Number of Cycles × Ah-throughput per cycle.

Table 5
Model comparison for key aging factors captured.

Key aging factors	ALST model	Semi-empirical model	Regression model
Temperature	Captured	Captured	Captured
Calendar	Captured	Captured	Not captured
Average SOC	Captured	Captured	Not captured
High C-rate	Captured	Not captured	Not captured
DOD	Not captured	Captured	Not captured

percentage error, and the regression model overpredicts the capacity loss by 42.7%. The ALST simulation result shows the best match with the experimental data.

3.5. Summary of the simulation results

Section 3 demonstrates that, as expected, the physics-based ALST model outperforms the semi-empirical and the empirical regression models. These results: (i) point to the merit of using experimentally validated physically-based models when possible, and (ii) demonstrate that semi-empirical and empirical models can underperform when used to predict under conditions that are not consistent with those originally used to generate or tune the models.

The key differences, in aging factors captured by each of the models, are summarized in Table 5.

The percentage error at the end point of the experimental data, predicted by each of the models across all four data sets, are summarized in Table 6. As shown, the ALST model has a percentage error of 10% or less for all four data sets. The regression model exhibits a percentage error 10% only when compared to the data used for calibration (data set 2), otherwise the error is between 20 and 60%. The semi-empirical model also performs poorly – 60 to 71% error – when compared to data sets not used for calibration, namely data sets 1 and 4. It is clear that from an accuracy point of view, the ALST model is preferred, however, the computational cost and complexity makes this model undesirable for system design or control algorithm development.

4. Conclusions

Three battery models, a 1-D electrochemical model (AutoLion ST, or ALST), a semi-empirical model (whose performance is predicted by an equivalent circuit model) and an empirical model (whose performance is predicted by an equivalent circuit model), are compared against each other as well as four published experimental data sets for a 2.3-Ah commercial graphite/$LiFePO_4$ cell. Key differences in the aging factors captured by each of the models are summarized. The physics-based ALST model (which predicts both performance and degradation) outperforms the other two models (for which the performance is predicted by an equivalent circuit model) across all four data sets, but is 20x slower than the empirical model, and 134x slower than the semi-empirical model. The semi-empirical and empirical models underperform when used for operating conditions that are not consistent with the data sets used for calibration. These findings are intended to help system designers and control engineers understand the strengths and weaknesses of these different types of models. More specifically, these results point to the lack of a physics-based and generalizable battery degradation model which is computationally fast and simple enough for use in model-based system design and algorithm development respectively.

5. Future work

Future efforts should include a focus on developing predictive battery degradation models that have the accuracy and computational complexity consistent with model-based control algorithm design and optimization-based powertrain sizing. As an example, in very recent work by some of the authors, a physically-based reduced-order degradation model for graphite anodes undergoing degradation via SEI layer growth and active material loss is outlined in Jin et al. (2017a).

Acknowledgments

This work is funded by the U.S. Department of Energy (grant no. DE-EE0005568), Purdue University and Cummins Inc. through the Hoosier Heavy Hybrid Center of Excellence. The authors are grateful to Prof. Edwin Garcia for helpful discussion and Dr. Kandler Smith, Dr. C. Delacourt and Dr. M. Safari for sharing the EV drive cycle data. The authors would also like to acknowledge the strategic direction and key inputs provided to this project by Vivek Sujan and Gary Parker from Cummins Inc.

Table 6
Model comparison for the accuracy (in percentage error).

Data sets	ALST model	Semi-empirical model	Regression model
Data set 1 (Spagnol et al., 2010)	6.4%	59.4%	20.5%
Data set 2 (Wang et al., 2011)	10.0%	10.0%	10.0%
Data set 3 (Safari & Delacourt, 2011a)	6.5%	29.3%	60.0%
Data set 4 (Nagpure, 2013)	4.5%	71.0%	42.7%

References

Delacourt, C., & Safari, M. (2012). Life simulation of a graphite/$LiFePO_4$ cell under cycling. *Journal of the Electrochemical Society*, *159*(8), A1283–A1291.

Fan, G., Pan, K., Canova, M., Marcicki, J., & Yang, X. G. (2016). Modeling of Li-ion cells for fast simulation of high c-rate and low temperature operations. *Journal of The Electrochemical Society*, *163*(5), A666–A676.

Forman, J. C., Bashash, S., Stein, J. L., & Fathy, H. K. (2011). Reduction of an electrochemistry-based Li-ion battery model via quasi-linearization and pade approximation. *Journal of the Electrochemical Society*, *158*(2), A93–A101.

Jin, X. (2017). *Physics-based computationally efficient battery degradation model and electric machine scaling strategy for hybrid electric vehicle design optimization*. Diss. Purdue University.

Jin, X., Vora, A., Hoshing, V., Saha, T., Shaver, G., García, R. E., et al. (2017a). Physically-based reduced-order capacity loss model for graphite anodes in Li-ion battery cells. *Journal of Power Sources*, *342*, 750–761.

Jin, X., Vora, A., Hoshing, V., Saha, T., Shaver, G., Wasynczuk, O., et al. (2017b). Comparison of Li-Ion battery degradation models for system design and control algorithm development. In *American control conference (ACC)* (pp. 74–79). IEEE.

Jin, X., Vora, A., Hoshing, V., Saha, T., Shaver, G., Wasynczuk, O., et al. (2017c). Physically-based reduced-order capacity loss model: SEI layer growth and active material loss for graphite anode. In *American control conference (ACC)* (pp. 80–85). IEEE.

Kalupson, J., Luo, G., & Shaffer, C. E. (2013). *SAE technical paper*. *AutoLion: A thermally coupled simulation tool for automotive Li-ion batteries, Tech. rep*.

Lawder, M. T., Northrop, P. W., & Subramanian, V. R. (2014). Model-based SEI layer growth and capacity fade analysis for EV and PHEV batteries and drive cycles. *Journal of The Electrochemical Society*, *161*(14), A2099–A2108.

Nagpure, S. C. (2013). Multi-scale characterization studies of aged Li-ion battery materials for improved performance. *Journal of the Electrochemical Society*, *16011*, A2111–A2154.

Niesony, A. (2009). Determination of fragments of multiaxial service loading strongly influencing the fatigue of machine components. *Mechanical Systems and Signal Processing*, *23*(8), 2712–2721.

Onori, S., Spagnol, P., Marano, V., Guezennec, Y., & Rizzoni, G. A new life estimation method for lithium-ion batteries in plug-in hybrid electric vehicles applications, *International Journal of Power Electronics* 4 (3).

Oswal, M., Paul, J., & Zhao, R. (2010). *A comparative study of lithium-ion batteries*. (pp. 2419–2430). University of Southern California.

Peterson, S. B., Apt, J., & Whitacre, J. (2010). Lithium-ion battery cell degradation resulting from realistic vehicle and vehicle-to-grid utilization. *Journal of Power Sources*, *195*(8), 2385–2392.

Ploehn, H. J., Ramadass, P., & White, R. E. (2004). Solvent diffusion model for aging of lithium-ion battery cells. *Journal of The Electrochemical Society*, *151*(3), A456–A462.

Prada, E., Di Domenico, D., Creff, Y., Bernard, J., Sauvant-Moynot, V., & Huet, F. (2013). A simplified electrochemical and thermal aging model of $LiFePO_4$-graphite Li-ion batteries: Power and capacity fade simulations. *Journal of The Electrochemical Society*, *160*(4), A616–A628.

Ramadesigan, V., Northrop, P. W., De, S., Santhanagopalan, S., Braatz, R. D., & Subramanian, V. R. (2012). Modeling and simulation of lithium-ion batteries from a systems engineering perspective. *Journal of The Electrochemical Society*, *159*(3), R31–R45.

Safari, M., & Delacourt, C. (2011a). Aging of a commercial graphite/$LiFePO_4$ cell. *Journal of the Electrochemical Society*, *158.10*, A1123–A1135.

Safari, M., & Delacourt, C. (2011b). Simulation-based analysis of aging phenomena in a commercial Graphite/$LiFePO_4$ cell. *Journal of the Electrochemical Society*, *158*(12), 1436–1447.

Safari, M., Morcrette, M., Teyssot, A., & Delacourt, C. (2009). Multimodal physics-based aging model for life prediction of Li-ion batteries. *Journal of the Electrochemical Society*, *156*(3), A145–A153.

Smith, K., Earleywine, M., Wood, E., Neubauer, J., & Pesaran, A. (2012). *SAE technical paper*. *Comparison of plug-in hybrid electric vehicle battery life across geographies and drive cycles*. No. 2012-01-0666.

Smith, K., Markel, T., & Pesaran, A. PHEV Battery Trade-Off Study and Standby Thermal Control, In 26th international battery seminar & exhibit.

Smith, K. A., Rahn, C. D., & Wang, C.-Y. (2008). Model order reduction of 1D diffusion systems via residue grouping. *Journal of Dynamic Systems, Measurement, and Control*, *130*(1), 011012.

Smith, K., & Wang, C.-Y. (2006). Solid-state diffusion limitations on pulse operation of a lithium ion cell for hybrid electric vehicles. *Journal of Power Sources*, *161*(1), 628–639.

Smith, K., Wood, E., Santhanagopalan, S., Kim, G., Neubauer, J., & Pesaran, A. Models for battery reliability and lifetime, In: *Battery congress*, April, 2013, (pp. 15–16).

Spagnol, P., Onori, S., Madella, N., Guezennec, Y., & Neal, J. (2010). Aging and characterization of Li-ion batteries in a HEV application for lifetime estimation. *IFAC Proceedings*, *437*, 186–191.

Subramanian, V. R., Diwakar, V. D., & Tapriyal, D. (2005). Efficient macro-micro scale coupled modeling of batteries. *Journal of The Electrochemical Society*, *152*(10), A2002–A2008.

Vora, A. P., Jin, X., Hoshing, V., Guo, X., Shaver, G., Tyner, W., et al. (2015). Simulation framework for the optimization of HEV design parameters: Incorporating battery degradation in a lifecycle economic analysis. *IFAC-PapersOnLine*, *48*(15), 195–202.

Vora, A., Jin, X., Hoshing, V., Saha, T., Shaver, G., García, R. E., et al. (2017). Design-space exploration of series plug-in hybrid electric vehicles for medium-duty truck applications in a total cost-of-ownership framework. *Journal of Applied Energy*, *202C*, 662–672.

Wang, J., Liu, P., Hicks-Garner, J., Sherman, E., Soukiazian, S., Verbrugge, M., et al. (2011). Cycle-life model for graphite-$LiFePO_4$ cells. *Journal of Power Sources*, *196*(8), 3942–3948.